Supplementary Information

Phase-segregation free Quasi-2D Perovskite/Organic Tandem Solar Cells with Low V_{OC} Loss and Efficiency beyond 21%

Haotian Wu,[a] Tianyi Chen,[a] Yaokai Li,[a] Shitao Guan,[a] Lin Zhang,[a] Tingjun Chen,[a] Yang Liu,[b] Yizheng Jin,[b] Lijian Zuo,[a] Weifei Fu,*[a] Gang Wu,*[a] Hongzheng Chen,*[a]

[a] MOE Key Laboratory of Macromolecular Synthesis and Functionalization, State Key Laboratory of Silicon Materials, Department of Polymer Science and Engineering, Zhejiang University, Hangzhou 310027, P. R. China

[b] Key Laboratory of Excited-State Materials of Zhejiang Province, State Key Laboratory of Silicon Materials, Department of Chemistry, Zhejiang University, Hangzhou, China

* Corresponding Authors.
e-mail: zjufwf@zju.edu.cn; wmang@zju.edu.cn; hzchen@zju.edu.cn

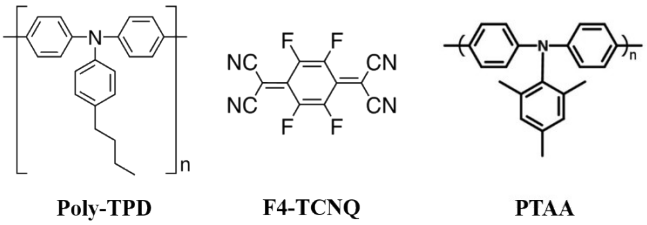

Figure S1. Schematic structure of Poly-TPD, F4-TCNQ and PTAA.

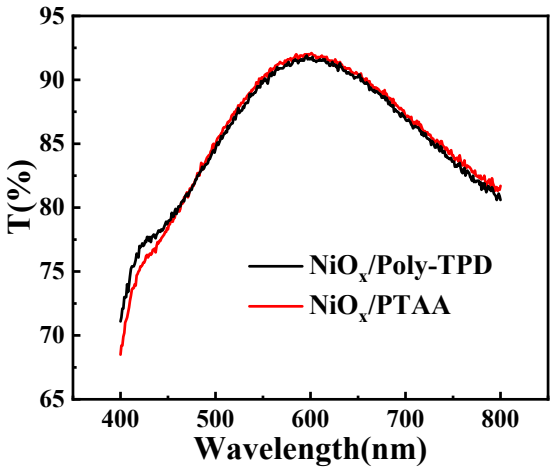

Figure S2. Transmission spectra of ITO glass coated by NiO_x/PTAA or NiO_x/Poly-TPD.

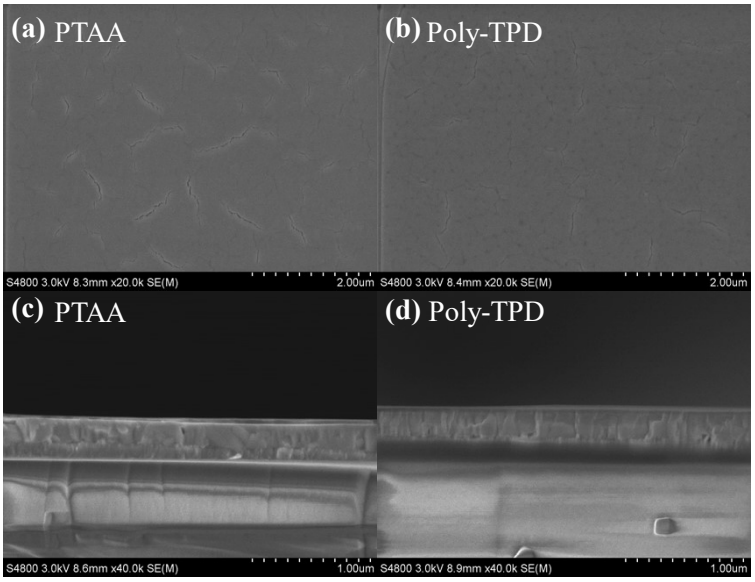

Figure S3. Top-view (a, b) and cross-sectional (c, d) SEM images of the $BA_{1.8}PEA_{0.2}MA_3Pb_4I_{13}$ films deposited on different substrate.

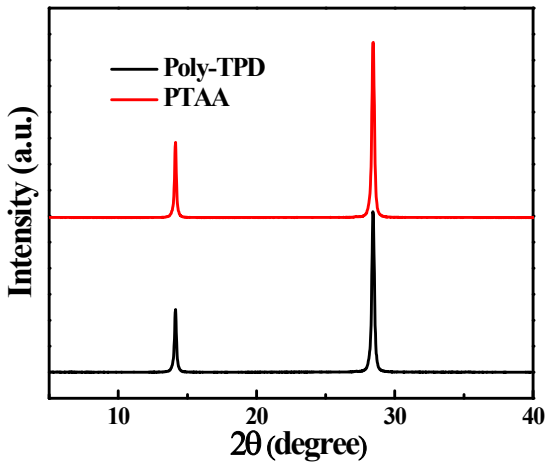

Figure S4. X-ray diffraction patterns of $BA_{1.8}PEA_{0.2}MA_3Pb_4I_{13}$ films deposited on different substrate.

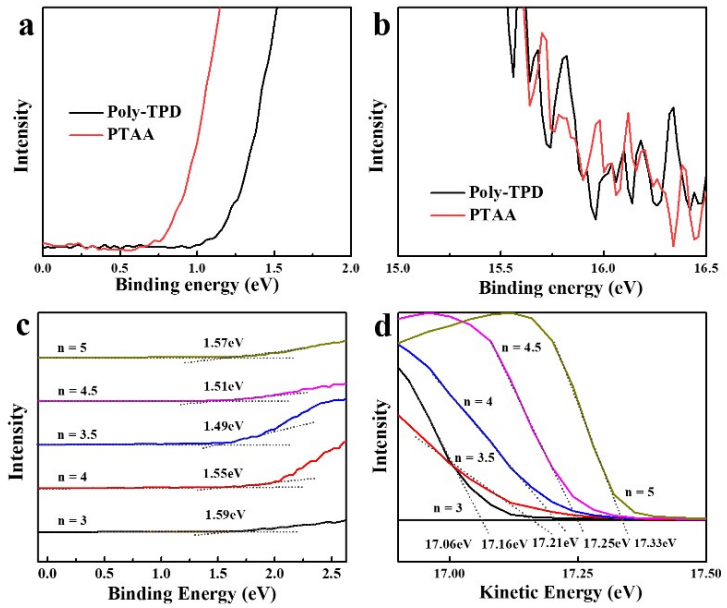

Figure S5. The UPS spectra of Poly-TPD, PTAA modified NiOx film (a), (b) and $BA_{1.8}PEA_{0.2}MA_{n-1}Pb_nI_{3n+1}$ film deposited on NiOx/Poly-TPD (c), (d).

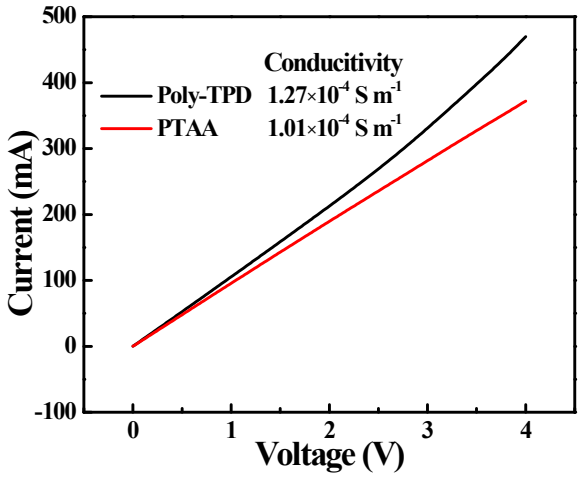

Figure S6. *I-V* curves of the devices with structure of ITO/modified NiO_x/Au.

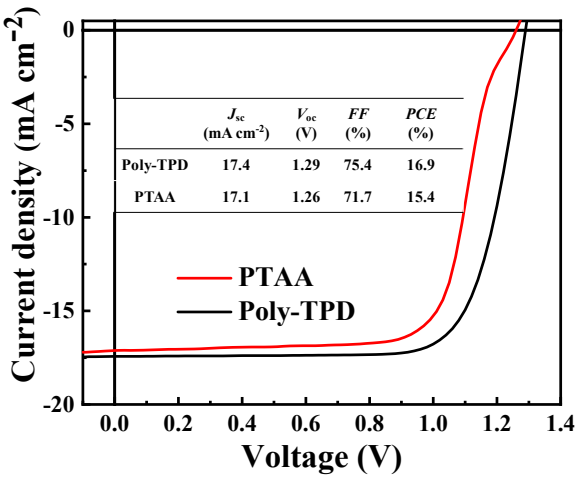

Figure S7. *J-V* curves and photovoltaic parameters of the $BA_{1.8}PEA_{0.2}MA_3Pb_4I_{13}$ PSC devices based on PTAA and Poly-TPD modified NiO_x under AM1.5G (100 mW cm^{-2}) illumination.

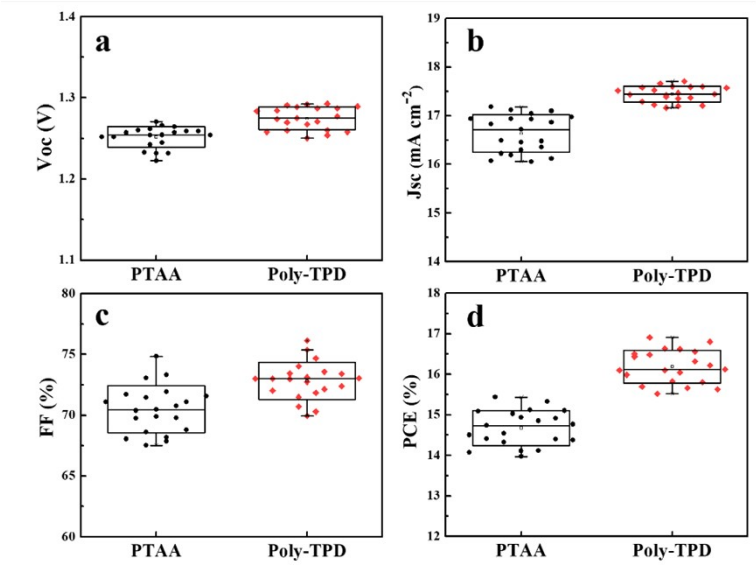

Figure S8. Distribution of V_{oc} (a), J_{sc} (b) , *FF* (c) and *PCE* (d) for $BA_{1.8}PEA_{0.2}MA_3Pb_4I_{13}$ PSC devices based on PTAA and Poly-TPD.

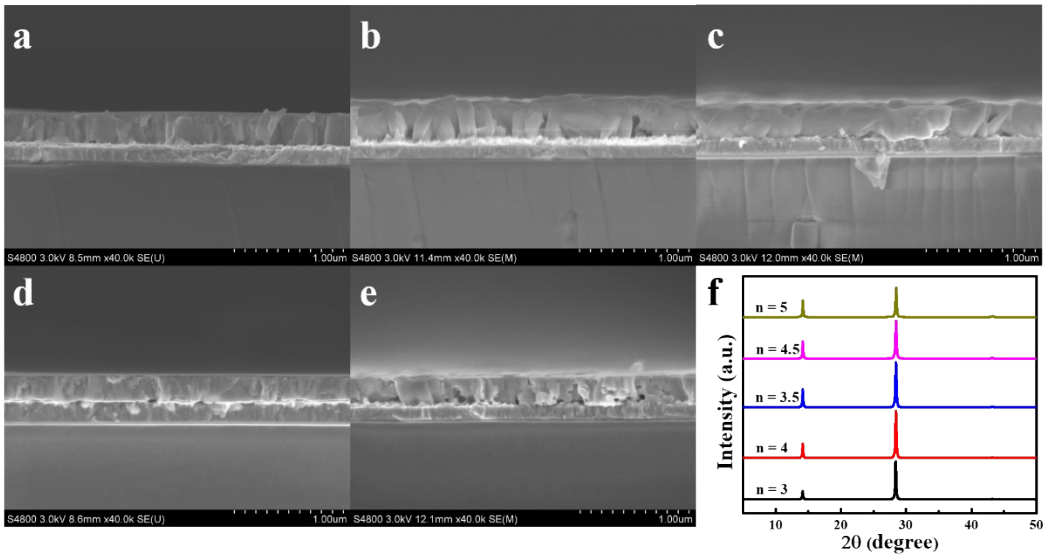

Figure S9. Cross-sectional SEM images and X-ray diffraction (XRD) patterns of $BA_{1.8}PEA_{0.2}MA_{n-1}Pb_nI_{3n+1}$ films deposited on Poly-TPD.

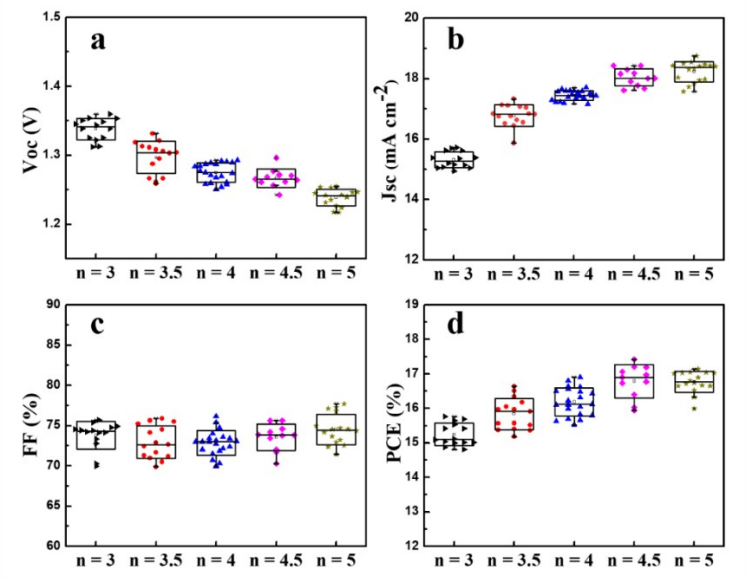

Figure S10. Distribution of V_{oc} (a), J_{sc} (b) , *FF* (c) and *PCE* (d) for $BA_{1.8}PEA_{0.2}MA_{n-1}Pb_nI_{3n+1}$ PSC devices deposited on Poly-TPD.

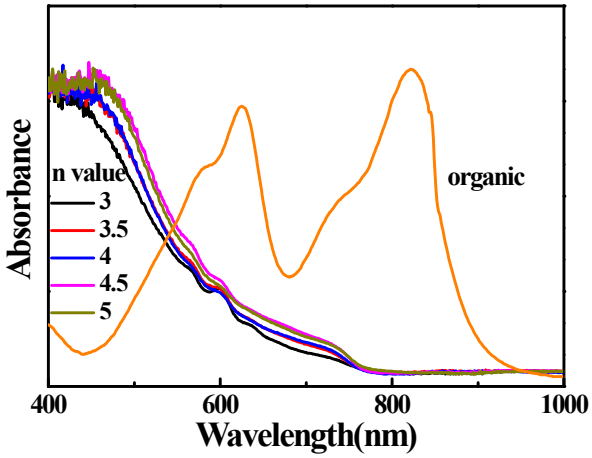

Figure S11. UV-Vis absorption spectra of $BA_{1.8}PEA_{0.2}MA_{n-1}Pb_nI_{3n+1}$ and PM6:BTP-eC9 film.

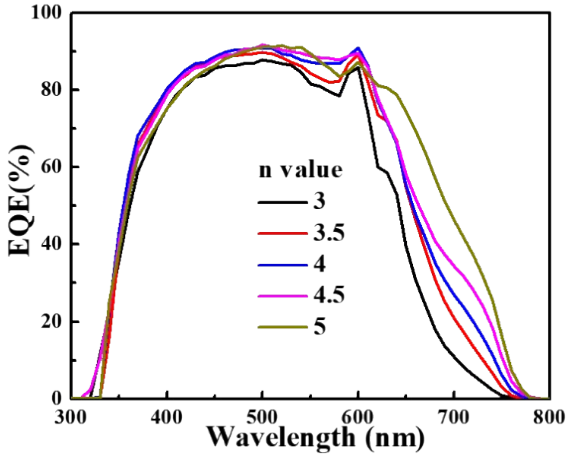

Figure S12. EQE spectra of $BA_{1.8}PEA_{0.2}MA_{n-1}Pb_nI_{3n+1}$ PSC devices deposited on Poly-TPD.

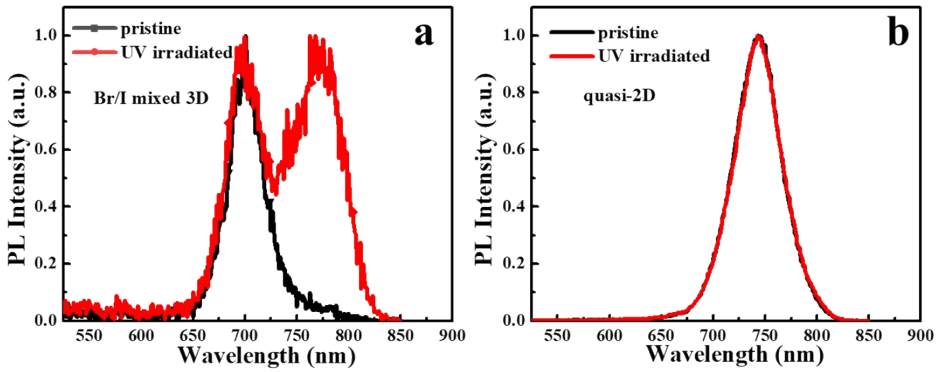

Figure S13. PL characteristics of the perovskite film before and after 470 nm UV irradiation. (a) Br/I mixed 3D perovskite under 15 min UV irradiation; (b) quasi-2D perovskite under 35min UV irradiation.

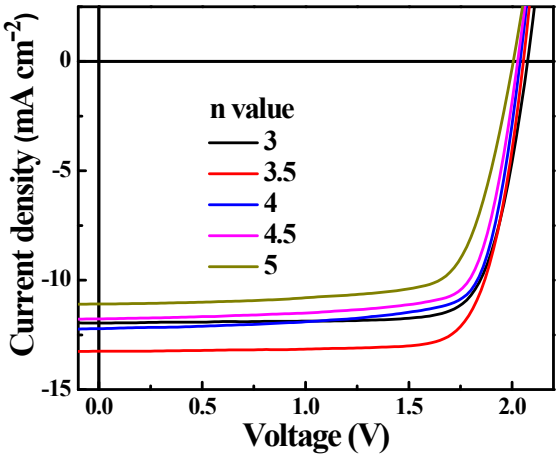

Figure S14. *J-V* curves of quasi-2D perovskite/organic TSCs based on $BA_{1.8}PEA_{0.2}MA_{n-1}Pb_nI_{3n+1}$ of different n value under AM1.5G (100 mW cm^{-2}) illumination.

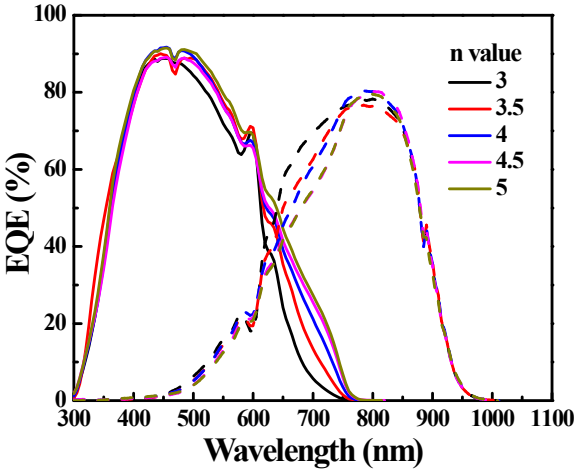

Figure S15. EQE curves of quasi-2D perovskite/organic TSCs based on $BA_{1.8}PEA_{0.2}MA_{n-1}Pb_nI_{3n+1}$ of different n value under AM1.5G (100 mW cm^{-2}) illumination.

Supplementary Text Note 1

Photovoltage estimation of $V_{oc,limit}$, V_{OC}^{SQ}, ΔV_{OC}^{rad} [1]:

$$V_{oc,limit} = V_{oc}^{SQ} - \Delta V_{oc}^{SQ} - \Delta V_{oc}^{rad} - \Delta V_{oc}^{nonrad}$$

$$V_{oc}^{SQ} = \frac{K_B T}{q} ln(\frac{J_{SC}^{SQ}}{J_0^{SQ}} + 1)$$;

$$\Delta V_{oc}^{SQ} = \frac{K_B T}{q} ln(\frac{J_{SC}^{SQ}}{J_{SC}})$$;

$$J_{SC}^{SQ} = q\int_{Eg}^{\infty} \emptyset_{AM1.5}(E)dE \quad ;$$

$$J_0^{SQ} = q\int_{Eg}^{\infty} \emptyset_{bb}(E)dE \quad ;$$

$$J_{SC} = q\int_0^{\infty} Q_e(E)\emptyset_{AM1.5}(E)dE \quad ;$$

$$\emptyset_{bb}(E) = \frac{\frac{2\pi E^2}{h^3c^2}}{exp\left(\frac{E}{K_BT}\right)1} - \approx \frac{2\pi E^2}{h^3c^2} exp(\frac{-E}{K_BT}) \quad ;$$

$$\Delta V_{oc}^{rad} = \frac{K_BT}{q} ln(\frac{J_0^{rad}}{J_0^{SQ}}) \quad ;$$

$$J_0^{rad} = q\int_0^{\infty} Q_e(E)\emptyset_{bb}(E)dE$$

$$\Delta V_{oc}^{nonrad} = \frac{K_BT}{e} \ln EQE_{EL}^{-1} \quad ;$$

where q, K_B, h, c, Eg is the elementary charge, Boltzmann constant, Planck constant, light speed in the vacuum and the bandgap of perovskite, respectively. V_{oc}^{SQ} is the Shockley-Queisser limit of open circuit voltage, ΔV_{oc}^{SQ} is the loss component related to non-ideal $Q_e(E)$. ΔV_{oc}^{rad} is the V_{oc} loss related to the sub-bandgap radiative recombination.With the assumption of no sub-bandgap region is extended, $Q_e(E)$ is given by the equation of:

$$Q_e(E) = \begin{cases} 0, & E < Eg \\ 0.9, & E \geq Eg \end{cases}$$

Then the ΔV_{oc}^{rad} for all n-value perovsktie was calculated to be 2.7meV. ΔV_{oc}^{nonrad} is the V_{oc} loss resulted from non radiative recombination. The bandgap of different n value 2D perosvkite could be obtained from the emission peak of the PL spectrum. $\emptyset_{bb}(E)$, $\emptyset_{AM1.5}(E)$ is solar cell radiative spectrum and black-body radiative spectrum,

respectively, which is shown in Figure S16. $J_{SC}^{SQ}, J_{0}^{SQ}, and\ J_{0}^{rad}$ is short-circuit current in S-Q limit, dark saturation current in S-Q limit and dark saturation current considering insuffient photon utilization and no extra EQE extending.

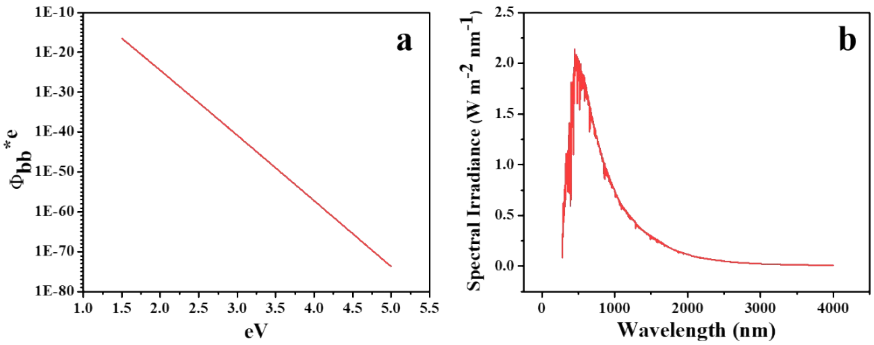

Figure S16. (a) The black body spectrum ϕBB*e at 300 K, (b) AM1.5G spectra.

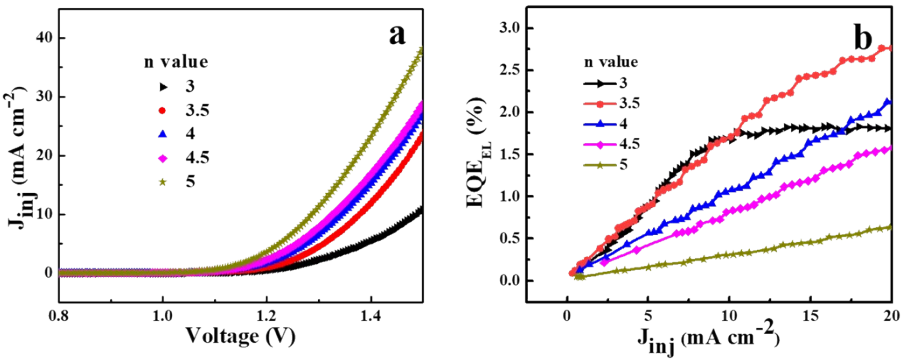

Figure S17. (a) Injection current of $BA_{1.8}PEA_{0.2}MA_{n-1}Pb_nI_{3n+1}$ perovskite devices in light-emitting diode (LED) mode under different voltages. (b) EQE_{EL} values of the devices with various injection current.

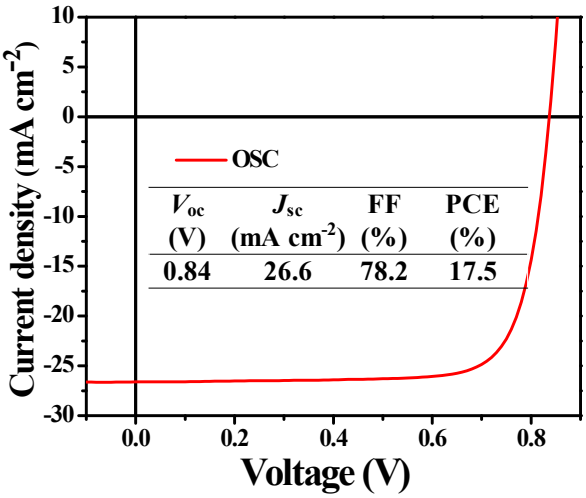

Figure S18. J-V curve and photovoltaic parameters of the OSC device.

Table S1. Summary of the photovoltaic parameters of reported perovskite/organic TSCs.

Structure	Front Subcell				PCE (%)	Stability	Ref
	Eg (eV)	Voc (V)	Voc loss (V)	PCE (%)			
ITO/Poly-TPD/$MA_{0.96}FA_{0.1}PbI_2Br(SCN)_{0.12}$/$PC_{61}BM$/BCP/Au/$MoO_3$/PM6:CH1007/PFN-Br/Ag	1.72	1.19	0.53	17.4	21.2	N_2, unencapsulated MPP: T90=75h	2
ITO/2PACZ/$FA_{0.6}MA_{0.4}Pb(I_{0.6}Br_{0.4})_3$/$C_{60}$/BCP/Ag/MoOx/PTB7-Th:BTPV-4Cl-eC9/PDINN/Ag	1.79	1.25	0.54	17.6	22.0	N_2, 25°C, UV light soaking T85=720h	3
ITO/SnO_2/$CsPbI_{1.8}Br_{1.2}$/PBDB-T/MoO_3/Au/ZnO/PFN/PM6:Y6/MoO3/Al	1.94	1.22	0.72	13.37	21.0	N_2, 25°C MPP: T91=1000h	4
ITO/(NiO_x/BPA)/$Cs_{0.25}FA_{0.75}Pb(I_{0.6}Br_{0.4})_3$/$C_{60}$/BCP/IZO/$MoO_3$/PM6:Y6:$PC_{71}BM$/PNDIT-F3N/Ag	1.79	1.26	0.53	17.8	23.6	N_2, capsulated, MPP: T90=500h	5
ITO/(NiO_x/MeO-2PACZ)/$FA_{0.8}Cs_{0.2}Pb(I_{0.5}Br_{0.5})_3$/$PC_{61}BM$/AZO-NP/ALD-$SnO_x$/ALD-$InO_x$/$MoO_3$/PM6:Y6:PC61BM/$C_{60}$/BCP/Ag	1.85	1.34	0.51	16.8	24.0	N_2 MPP: T80=100h	6
ITO/ZnO/SnO_2/$CsPbI_2Br$/PDCBT/MoO_3/Ag/ZnO/PM6:Y6/MoO_3/Ag	1.9	1.27	0.63	14.5	18.4	/	7
ITO/NiO_x/$FA_{0.8}MA_{0.02}Cs_{0.18}PbI_{1.8}Br_{1.2}$/$C_{60}$/BCP/Ag/MoO3/PBDBT-2F:Y6:$PC_{71}BM$/TPBi/Ag	1.77	1.11	0.66	14.1	20.6	N_2 MPP: T100=100h	8
ITO/NiO_x/Poly-TPD/$BA_{1.8}PEA_{0.2}MA_{2.5}Pb_{3.5}I_{11.5}$/$PC_{61}BM$/BCP/Au/MoOx/PM6:BTP-eC9/PFN/Ag	1.71	1.32	0.39	16.6	21.3	RH=50-80%, ambient, capsulation, MPP: T90>500h	This work

Table S2. Photovoltaic parameters of reported quasi-2D PSCs.

Structure	V_{oc} (V)	J_{sc} (mA cm^{-2})	*FF* (%)	PCE (%)	Eg (eV)	V_{oc} loss (V)	Ref.
ITO/(NiO_x/PTAA)/ (3AMP)($MA_{0.75}FA_{0.25}$)$_3Pb_4I_{13}$/ $PC_{61}BM$/BCP/Ag	1.24	19.51	77.27	18.67	1.59	0.35	9
ITO/PTAA/ $AA_2MA_4Pb_5I_{16}$/C_{60}/BCP/Ag	1.24	18.69	79.13	18.34	1.65	0.41	10
ITO/PTAA/$(4FPEA)_2(MA)_4Pb_5I_{16}$/ $PC_{61}BM$/PEI/Ag	1.16	19.00	78.98	17.34	1.61	0.45	11
ITO/PTAA//$(PEA)_2(MA)_4Pb_5I_{16}$/ $PC_{61}BM$/PEI/Ag	1.22	17.91	82.4	18.04	1.68	0.46	12
ITO/PEDOT:PSS/$(ThMA)_2(FA)_4Pb_5I_{16}$/$PC_{61}BM$/BCP/Ag	1.08	23.39	75.8	19.06	1.50	0.42	13
ITO/PEDOT:PSS/$(NpMA)_2(MA)_3Pb_4I_{13}$/$PC_{61}BM$/BCP/Ag	1.24	20.89	66.35	17.25	1.62	0.38	14
ITO/PTAA/$(4FPEA)_2(FA)_4Pb_5I_{16}$/ $PC_{61}BM$/BCP/Au	1.18	22.45	79.53	21.07	1.54	0.36	15
ITO/PEDOT:PSS/$(ThFA)_2(MA)_2Pb_3I_{10}$/PM6:Y6:$PC_{61}BM$/BCP/Ag	1.12	23.07	73.82	19.15	1.61	0.49	16
ITO/PTAA/$(F\text{-}PEA)_2(MA)_3Pb_4I_{13}$/ $PC_{61}BM$/PEI/Ag	1.21	19.04	78.5	18.1	1.63	0.42	17
ITO/PEDOT:PSS/$(PEA)_2(MA)_3Pb_4I_{13}$/$PC_{61}BM$/BCP/Ag	1.20	18.52	83.39	18.48	1.65	0.45	18
ITO/PTAA/$AA_2MA_3Pb_4I_{13}$/C_{60}/BCP/Ag	1.24	18.57	80.29	18.42	1.60	0.36	19

Table S3. Summary of the photovoltaic parameters for the $BA_{1.8}PEA_{0.2}MA_{n-1}Pb_nI_{3n+1}$ PSC devices based on NiO_x/poly-TPD under AM1.5G (100 mW cm^{-2}) illumination.

n	V_{oc} (V)	J_{sc} (mA cm^{-2})	FF (%)	$PCE_{max/ave}$ (%)	V_{oc} loss (V)
3	1.35	15.2	75.4	15.4/14.4	0.38
3.5	1.32	16.6	75.9	16.6/15.0	0.39
4	1.29	17.4	75.4	16.9/16.2	0.40
4.5	1.27	18.2	74.6	17.2/16.4	0.41
5	1.26	18.3	74.7	17.1/16.4	0.41

Table S4. Values of EQE_{EL} and calculated ΔV_{oc}^{nonrad}, ΔV_{oc}^{rad}, ΔV_{oc}^{SQ}, $V_{oc,\ limit}$ of the quasi-2D PSCs with different n value.

n value	EQE_{EL} (%)	V_{oc}^{SQ} (V)	ΔV_{oc}^{nonrad} (V)	ΔV_{oc}^{rad} (V)	ΔV_{oc}^{SQ} (V)	$V_{oc,\ limit}$ (V)
3	1.797	1.45	0.104	0.0027	0.006578	1.34
3.5	2.485	1.42	0.096	0.0027	0.005079	1.32
4	1.903	1.41	0.103	0.0027	0.004368	1.30
4.5	1.487	1.40	0.109	0.0027	0.003579	1.28
5	0.556	1.39	0.134	0.0027	0.003684	1.25

Table S5. Photovoltaic parameters of the OSC device under AM1.5G (100 mW cm^{-2}) illumination.

V_{oc} (V)	J_{sc} (mA cm^{-2})	FF (%)	PCE (%)
0.84	26.6	78.2	17.5

Table S6. The highest calculated J_{sc} for quais-2D perovskite/organic TSCs with different n value and the corresponding thickness of the active layer for front/rear subcells.

n value	Film Thickness (nm)		J_{sc} (mA cm^{-2})
	organic	perovskite	
3	100	460	14.8
3.5	120	420	15.4
4	120	340	15.4
4.5	140	300	15.3
5	140	260	15.3

Reference

1. Li, Z. *et al.* Organometallic-functionalized interfaces for highly efficient inverted perovskite solar cells. *Science* **376**, 416–420 (2022).
2. Xie, Y.-M. *et al.* Homogeneous Grain Boundary Passivation in Wide-Bandgap Perovskite Films Enables Fabrication of Monolithic Perovskite/Organic Tandem Solar Cells with over 21% Efficiency. *Adv. Funct. Mater.* **n/a**, 2112126 (2022).
3. Qin, S. *et al.* Constructing Monolithic Perovskite/Organic Tandem Solar Cell with Efficiency of 22.0% via Reduced Open-circuit Voltage Loss and Broadened Absorption Spectra. *Adv. Mater.* **n/a**, 2108829 (2022).
4. Chen, W. *et al.* Surface Reconstruction for Stable Monolithic All-Inorganic Perovskite/Organic Tandem Solar Cells with over 21% Efficiency. *Adv. Funct. Mater.* **32**, 2109321 (2022).
5. Chen, W. *et al.* Monolithic perovskite/organic tandem solar cells with 23.6% efficiency enabled by reduced voltage losses and optimized interconnecting layer. *Nat. Energy* 1–9 (2022) doi:10.1038/s41560-021-00966-8.
6. Brinkmann, K. O. *et al.* Perovskite–organic tandem solar cells with indium oxide interconnect. *Nature* **604**, 280–286 (2022).
7. Xie, S. *et al.* Efficient monolithic perovskite/organic tandem solar cells and their efficiency potential. *Nano Energy* **78**, 105238 (2020).
8. Chen, X. *et al.* Efficient and Reproducible Monolithic Perovskite/Organic Tandem Solar Cells with Low-Loss Interconnecting Layers. *Joule* **4**, 1594–1606 (2020).
9. Wu, H. *et al.* Merged interface construction toward ultra-low Voc loss in inverted two-dimensional Dion–Jacobson perovskite solar cells with efficiency over 18%. *J. Mater. Chem. A* (2021) doi:10.1039/d1ta02015c.
10. Li, K. *et al.* High Efficiency Perovskite Solar Cells Employing Quasi-2D Ruddlesden-Popper/Dion-Jacobson Heterojunctions. *Adv. Funct. Mater.* **n/a**, 2200024 (2022).
11. Shi, J. *et al.* Fluorinated Low-Dimensional Ruddlesden–Popper Perovskite Solar Cells with over 17% Power Conversion Efficiency and Improved Stability. *Adv. Mater.* **31**, 1901673 (2019).
12. Zhang, J. *et al.* Uniform Permutation of Quasi-2D Perovskites by Vacuum Poling for Efficient, High-Fill-Factor Solar Cells. *Joule* **3**, 3061–3071 (2019).
13. Lai, H. *et al.* Organic-Salt-Assisted Crystal Growth and Orientation of Quasi-2D Ruddlesden–Popper Perovskites for Solar Cells with Efficiency over 19%. *Adv. Mater.* **32**, 2001470 (2020).
14. Xu, Z. *et al.* Phase Distribution and Carrier Dynamics in Multiple-Ring Aromatic Spacer-Based Two-Dimensional Ruddlesden–Popper Perovskite Solar Cells. *ACS Nano* **14**, 4871–4881 (2020).
15. Shao, M. *et al.* Over 21% Efficiency Stable 2D Perovskite Solar Cells. *Adv. Mater.* **n/a**, 2107211 (2021).
16. Wang, T. *et al.* Integrated Quasi-2D Perovskite/Organic Solar Cells with Efficiency over 19% Promoted by Interface Passivation. *Adv. Funct. Mater.* **n/a**, 2107129 (2021).
17. Wang, Z. *et al.* Spacer Cation Tuning Enables Vertically Oriented and Graded Quasi-2D Perovskites for Efficient Solar Cells. *Adv. Funct. Mater.* **n/a**, 2008404 (2021).
18. Yang, Y. *et al.* Defect Suppression in Oriented 2D Perovskite Solar Cells with Efficiency over 18% via Rerouting Crystallization Pathway. *Adv. Energy Mater.* **11**, 2002966 (2021).
19. Wu, G. *et al.* Molecular Engineering for Two-Dimensional Perovskites with Photovoltaic Efficiency Exceeding 18%. *Matter* **4**, 582–599 (2021).